ISTANBUL TECHNICAL UNIVERSITY ★ GRADUATE SCHOOL

SELF-SUPERVISED DEEP CONVOLUTIONAL NEURAL NETWORK TRAINING FOR LOW-DOSE CT RECONSTRUCTION

M.Sc. THESIS

Mehmet Ozan ÜNAL

Department of Electronics and Communication Engineering

Biomedical Engineering Programme

JANUARY 2022

ISTANBUL TECHNICAL UNIVERSITY ★ GRADUATE SCHOOL

SELF-SUPERVISED DEEP CONVOLUTIONAL NEURAL NETWORK TRAINING FOR LOW-DOSE CT RECONSTRUCTION

M.Sc. THESIS

Mehmet Ozan ÜNAL
(504181414)

Department of Electronics and Communication Engineering

Biomedical Engineering Programme

Thesis Advisor: Assoc. Prof. Dr. İsa YILDIRIM

JANUARY 2022

İSTANBUL TEKNİK ÜNİVERSİTESİ ★ LİSANSÜSTÜ EĞİTİM ENSTİTÜSÜ

DÜŞÜK DOZLU BT GERİÇATMASI İÇİN DERİN EVRİŞİMLİ SİNİR AĞLARININ ÖZ DENETİMLİ EĞİTİMİ

YüKSEK LİSANS TEZİ

Mehmet Ozan ÜNAL
(504181414)

Elektronik ve Haberleşme Mühendisliği Anabilim Dalı

Biyomedikal Mühendisliği Programı

Tez Danışmanı: Assoc. Prof. Dr. İsa YILDIRIM

OCAK 2022

Mehmet Ozan ÜNAL, a M.Sc. student of ITU Graduate School student ID 504181414, successfully defended the thesis entitled "SELF-SUPERVISED DEEP CONVOLUTIONAL NEURAL NETWORK TRAINING FOR LOW-DOSE CT RECONSTRUCTION", which he prepared after fulfilling the requirements specified in the associated legislations, before the jury whose signatures are below.

Thesis Advisor :	**Assoc. Prof. Dr. İsa YILDIRIM** Istanbul Technical University	.....
Jury Members :	**Prof. Dr. Gözde ÜNAL** Istanbul Technical University	.....
	Assoc. Prof. Dr. Esin Öztürk IŞIK Boğaziçi University	.....

Date of Submission : 14 Jan 2022
Date of Defense : 11 Feb 2022

To my family

FOREWORD

This thesis was written for my MSc. degree in Biomedical Engineering Programme at Istanbul Technical University, Turkey. In this study, a new self-supervised training scheme is proposed for low-dose CT reconstruction which uses only low-dose projections without the need for low-dose/normal-dose pairs. This is a crucial research topic in terms of creating new potential usage of deep learning in the field with self-supervised training.

I would like to thank a few people here. I am really grateful to my advisor, Assoc. Prof. Dr. Isa Yildirim, who has been leading me every step of this study and help me to understand how to become a good researcher and engineer. I would like to thank Dr. Metin Ertaş who guide me to improve my abilities and my theoretical understandings of inverse imaging problems. Working with them was an amazing learning and applying journey and this study was not possible without their collaboration.

January 2022 Mehmet Ozan ÜNAL

TABLE OF CONTENTS

Page

ABBREVIATIONS

BM3D : Block Matching 3D
CNN : Convolutional Neural Network
CT : Computerized Tomography
DNN : Deep Neural Network
FBP : Filtered Back Projection
SART : Simultaneous Algebraic Reconstruction Technique
TV : Total Variation

LIST OF TABLES

Page

LIST OF FIGURES

Page

SELF-SUPERVISED
DEEP CONVOLUTIONAL NEURAL NETWORK TRAINING
FOR LOW-DOSE CT RECONSTRUCTION

SUMMARY

Computed tomography (CT) is a medical imaging technique to obtain a noninvasively three-dimensional image of the body. CT imaging is one of the most crucial tools which is used for monitoring the human body and diagnosing serious illnesses. In CT imaging, one of the most serious concerns has been ionizing radiation since exposure to large amounts of radiation can cause serious illnesses.

Various low-dose CT reconstruction approaches have been proposed to reduce the dose level without compromising image quality. With the emergence of deep learning, the increasing availability of computational power, and huge datasets, data-driven methods have recently gotten a lot of attention. Deep learning-based methods have also been applied in various ways to address low-dose CT reconstruction problem. However, the success of these methods is usually dependent on labeled data, which requires tedious work by radiologists for CT imaging.

Recent studies, however, have also shown that training may be done successfully with noisy datasets without the requirement of noise-free target data. In this study, a training scheme is defined to use low-dose projections as their own training targets. We apply the self-supervision principle in the projection domain where the noise is element-wise independent, which is a requisite for self-supervised training methods. The parameters of a denoiser neural network are optimized through self-supervised training.

Experiments are done with both analytical and human CT data. Slices from deep lesion dataset for human CT data and ellipses dataset for synthetic data are used. To simulate low-dose settings, 64 views parallel beam geometry is used. The noisy projections are created with additive white Gaussian noise with 30, 33, and 37 dB SNR values. The proposed method is compared with FBP, SART, SART+TV, SART+BM3D, and the supervised FBP+U-Net method. The methods are compared quantitatively with PSNR and SSIM metrics, and the reconstructions are qualitatively assessed regarding background smoothness, the sharpness of the details, and the recoverability of the lesions with some visual examples.

In the comparisons, it is shown that the proposed method outperforms both traditional and compressed sensing-based iterative reconstruction methods in the reconstruction of analytic CT phantoms and real-world CT images in the low-dose CT reconstruction task, both qualitatively and quantitatively. Besides, it produces comparable results with the supervised approach.

DÜŞÜK DOZLU BT GERİÇATMASI İÇİN DERİN EVRİŞİMLİ SİNİR AĞLARININ ÖZ DENETİMLİ EĞİTİMİ

ÖZET

Bilgisayarlı tomografi (BT), vücudun invaziv olmayan bir şekilde üç boyutlu görüntüsünü elde etmek için kullanılan tıbbi bir görüntüleme tekniğidir. BT görüntüleme sırasında radyasyon kaynağı, X ışınları yayarak sarmal bir yörüngede hasta etrafında döner ve farklı açılardaki dedektör verileri toplanır. Bu toplanan veriler BT projeksiyonları olarak bilinir ve bunlardan oluşturulan görüntü BT görüntüsü olarak bilinir. BT görüntüleme, insan vücudunudaki dokuları görüntülemek ve ciddi hastalıkları teşhis etmek için kullanılan en önemli araçlardan biridir. BT görüntülemede en ciddi endişelerden biri ise iyonlaştırıcı radyasyon olmuştur. Görüntü kalitesinden ödün vermeden doz seviyesini azaltmak için çeşitli düşük doz BT geri çatma yaklaşımları önerilmiştir.

Projeksiyonlar gürültülü veya eksik olduğunda, FBP yöntemi tatmin edici sonuçlar vermez. İlerleyen yıllarda farklı düşük doz BT görüntüleme koşullarında geri çatma kalitesini iyileştirmek için çeşitli yöntemler önerilmiştir. Düşük dozlu BT geri çatması için önerilen yöntemlerden biri, hatanın yinelemeli olarak geriye yansıtılmasıyla çalışan yinelemeli yöntemlerdir. En popüler yinelemeli yöntemlerden biri olan Simultaneous Algebraic Reconstruction Technique (SART), tüm projeksiyonlar için hatayı aynı anda geri yansıtır. Son zamanlarda, düşük doz BT geri çatma problemi için sıkıştırılmış algılama tabanlı yöntemler önerilmiştir. Sıkıştırılmış algılama teorisine göre, eğer bir bilgi bilinen bir uzayda seyrek ise, bu bilgi onun eksik ölçümleriyle yeniden oluşturulabilir. Doğal görüntüler genellikle seyrek değildir, ancak bir bilgi doğrusal bir dönüşüm yoluyla seyrekleştirilebiliyorsa, sıkıştırılmış algılama teorisi hala geçerlidir. Popüler bir doğrusal seyrekleştirme dönüşümü olan Toplam Varyasyon (TV) minimizasyonu, çözüm setini görüntülerin gradyan büyüklüğünü en aza indirmeyi amaçlayarak sınırlar. Sonraki yıllarda iteratif ve sıkıştırılmış algılama tabanlı yöntemler birleştirilmiş ve düşük doz BT geri çatma problemi için önerilmiştir.

Derin öğrenmenin ortaya çıkması, hesaplama gücünün artan kullanılabilirliği ve devasa veri kümeleri ile veriye dayalı yöntemler son zamanlarda büyük ilgi görmektedir. Derin öğrenmeye dayalı yöntemler, düşük dozlu BT geri çatma problemini çözmek için de çeşitli şekillerde uygulanmıştır. Görüntü uzayında, gürültü gidericiler olarak genellikle Evrişimli Sinir Ağı (CNN) tabanlı yaklaşımlar kullanılır. Derin öğrenme ayrıca yinelemeli geri çatma yöntemleriyle genişletilip ve yinelemeli olarak uygulanmıştır. Bununla birlikte, bu yöntemlerin başarısı genellikle etiketlenmiş verilere ve verisetlerinin büyüklüğüne bağlı durumdadır. Ancak son çalışmalar, gürültülü veri kümeleriyle, gürültüsüz hedef verilere gerek kalmadan derin sinir

ağlarının eğitiminin başarıyla yapılabileceğini göstermiştir. Noise2Noise temiz hedef görüntüleri gerektirmeyen bir gürültü giderme yöntemidir. Bu yöntemin çalışabilmesi için aynı bilginin iki farklı gürültülü ölçümü gereklidir. Noise2Self ve Noise2Void çalışmaları ise gürültü gidermenin sadece gürültülü ölçümün kendisi kullanılarak yapılabileceğini önermiş ve görüntü uzayı problemlerinde uygulamıştır.

Biz de bu çalışmada bu yöntemlere benzer şekilde, düşük doz projeksiyonları kendi eğitim hedefleri olarak kullanmak için bir eğitim şeması tanımladık. Öz denetimli öğrenme yöntemlerinin gerekliliklerinden biri de gürültünün pixeller arası bağımsız olmasıdır. Bu nedenle öz denetimli eğitim yöntemi gürültünün bu şekilde modellenebileceği projeksion uzayında uygulanmıştır. Gürültü giderici bir sinir ağının parametreleri, bu tanımladığımız öz denetimli eğitim yoluyla optimize edilmiştir. Önerilen geri çatma üç aşamada anlatılabilinir: Ön işleme, eğitim ve geri çatma. Ön işleme, Radon dönüşümü ve toplamsal beyaz Gauss gürültüsü kullanılarak CT görüntülerinden düşük dozlu projeksiyonlar oluşturmayı içerir. Elde edilen projeksiyon veri seti iki bölüme ayrılmıştır: eğitim ve test. Eğitim kümesi projeksiyonları için, piksellerin J. alt kümesi pertürbe edilir ve FBP geri çatma yöntemine giriş olarak verilir. Pertürbasyonlar için aşağıdaki adımlar kullanılır: 1. Giriş görüntüsünü kare parçalara bölmek için bir ızgara kullanılır. Bizim deney setimizde 4x4 olarak ayarlanmıştır. 2. Pertürbe edilecek piksel (i.), iterasyon sayısının ızgaradaki piksel sayısına (4x4=16) bölünmesiyle seçilir. Örneğin, yineleme sayısı 172 ise, 172 mod(16) = 12'dir. 3. Her ızgaranın i. pikseli, i. pikselinin kendisi hariç tutularak, bitişik dört pikselin ortalaması ile pertürbe edilir. FBP çıktısı, sinir ağı kullanılarak gürültüden arındırılır ve daha sonra Radon dönüşümü yoluyla projeksiyon uzayına iletilir. Hataya J. alt küme maskesini uyguladıktan sonra, çıktı ile pertürbe edilmiş projeksiyonlar arasında hata hesaplanır. Sinir ağı, tanımladğımız bu hatayı minimize etmek için Adam yöntemi kullanılarak optimize edilmiştir. Ağ ağırlıkları eğitim tarafından öğrenildikten sonra geri çatma için kullanılır. Geri çatma sırasında, girdi projeksiyonları hiçbir değişiklik yapılmadan ham formda FBP operatörüne iletilir. Geri çatılmış görüntü, öğrenilmiş parametreleri kullanak derin sinir ağı tarafından görültüden arındırılır.

Hem analitik hem de tıbbi BT verileri üzerinde deneyler yapılmıştır. İnsan CT verileri olarak, Deep Lesion veri setinden ve sentetik veri olarak elips veri setinden kesitler kullanılmıştır. Düşük doz ayarlarını simüle etmek için 64-açı paralel ışın geometrisi kullanılmıştır. Gürültülü projeksiyonlar, 30, 33 ve 37 dB SNR değerlerine sahip toplamsal beyaz Gauss gürültüsü ile oluşturulmuştur. Önerilen yöntem FBP, SART, SART+TV, SART+BM3D ve FBP+U-Net yöntemleri ile karşılaştırılmıştır. Yöntemler nicel olarak PSNR, SSIM metrikleri ile karşılaştırılırken, geri çatılan görüntülerden alınan bazı görsel örneklerle arka plan pürüzsüzlüğü, detayların keskinliği ve lezyonların geri kazanılabilirliği açısından niteliksel olarak değerlendirilmiştir. Tüm gürültü seviyeleri için FBP, bu kriterlere göre en kötü sonuçları vermiştir. SART'ın çıkış görüntüsü TV veya BM3D aracılığıyla gürültüden arındırıldığında performansı büyük ölçüde artar. Bu deney koşulları altında, denetimli yöntem en iyi sonucu verir. Görsel sonuçlarda ise bulgular şu şekildedir. FBP geri çatılmış görüntüsünde ciddi artefaktlar var. SART daha iyi sonuçlar verir, ancak yine de çok fazla arka plan gürültüsü vardır. TV ve BM3D arka plan gürültüsünü etkili bir şekilde bastırsa da, aşırı yumuşatma etkileri küçük detayların algılanabilirliğini azaltır. Önerilen öz denetimli yöntem ve denetimli yaklaşım, arka plan gürültüsünü azaltma ve ince ayrıntıları kurtarma açısından diğerlerinden daha iyi performans gösterir. Önerilen yöntem

ile denetimli yöntem arasında daha iyi niteliksel bir karşılaştırma için şekillerde yakınlaştırılmış alanlar kullanılmıştır, bu da önerilen yöntemin bir çok deney setinde denetimli yöntem ile karşılaştırılabilir sonuçlar verdiğini gösterir.

Sonuç olarak karşılaştırmalarımızda, yöntemimizin analitik BT fantomlarının ve gerçek dünya BT görüntülerinin geri çatmasında hem niteliksel hem de niceliksel olarak iyi performans göstediği sergilenmiştir. Hem geleneksel FBP methodundan hem de sıkıştırılmış algılama tabanlı yinelemeli geri çatma yöntemlerinden daha iyi performans gösterdiği ortaya konulmuştur.

1. INTRODUCTION

1.1 Problem Definition

Computerized Tomography (CT) is used to monitor the interior of the human body noninvasively. Problematic tissues, deformities, and lesions can be detected by CT scans. Despite these benefits, CT imaging has one crucial drawback: ionizing radiation. Researchers have been working to reduce the impact of this negativity for many decades by aiming to preserve image quality with lower radiation dose, which is also known as low-dose CT imaging. The radiation dose reduction of CT imaging is possible in three ways: *i*) reducing the number of viewing angles, *ii*) reducing of x-ray tube current. *iii*) narrowing down the viewing angle.

During CT imaging, the radiation source rotates around the patient in a helical trajectory by emitting x-rays, and the detector data at different angles is collected. These gathered data are known as CT projections, and the image created from them is known as a CT image. This data acquisition process is defined mathematically as follows:

$$y = Ax^* + \eta \tag{1.1}$$

where $x^* \in \mathbb{R}^n$ is the CT image, $y \in \mathbb{R}^m$ is the projections, and $A \in \mathbb{R}^{m \times n}$ is the forward projection operator, η is the noise which is formed during the projecting and measurements processes. CT reconstruction is the creation of images from these noisy indirect projections. Filtered Back Projection (FBP), the traditional method used in CT imaging, reconstructs a CT image by projecting CT projections back to the image domain. Since low frequencies are sampled more than high frequencies due to the system geometry, a filter is used to weight the impact of low frequencies while lowering the effect of high frequencies. However, this operation increases the sensitivity of FBP method to noise. Therefore, when the projections are noisy or incomplete, FBP method does not yield satisfactory results. Various methods are proposed to improve

the reconstruction quality for different low-dose CT imaging settings in the following years.

1.2 Related Work

One of the proposed methods for low-dose CT reconstruction is iterative methods which usually works by iterative backprojection of the error. Simultaneous Algebraic Reconstruction Technique (SART) [1], one of the most popular iterative method, simultaneously back-projects the error for all projections. Recently, compressed sensing based methods are proposed for low-dose CT reconstruction problem. According to compressed sensing theory, if an information is sparse on a known basis, this information can be recovered by its incomplete measurements [2, 3]. Natural images are not usually sparse however compressed sensing theory is still valid if an information can be sparsified via a linear transform. Total Variation (TV) minimization, a popular linear sparsifying transform, aims to minimize the gradient magnitude of the images, which constrains the solution set to piece-wise smooth images [4]. Iterative and compressed sensing based methods are combined and proposed for low-dose CT reconstruction problem in the following years [5, 6]. The image domain denoisers which exploit non-local similarities such as Non-Local means [7] and Block Matching 3D (BM3D) [8] are also applied to low-dose CT problem. Sparsifying transforms and dictionary learning techniques are utilized for the reconstruction and denosing of low-dose CT images. However, these methods are usually handcrafted and hyperparameter dependent.

With the development in processing capability and the availability of big data sets in the years afterwards, the number of deep learning based research is expanded. Many deep learning based approaches for image domain inverse problems such as denoising, deconvolution, and inpainting have been presented. Deep learning algorithms have also been used to solve the low-dose CT problem. In the image domain, Convolutional Neural Network (CNN) based approaches are utilized as denoisers [9–13]. Deep learning is also extended with iterative reconstruction methods and used iteratively with traditional reconstruction approaches [14–16]. The availability of big data sets is one of the most crucial criteria in the success of these data-driven methods [17].

Noise2Noise [18] offers an approach for the denoising problem that does not require noise-free target images. The denoising method is attempted to be learned by employing two distinct noisy measurements of the same information. Noise2Noise approach still needs two separate noisy measurements of the information. Noise2Self [19] and Noise2Void [20] studies, on the other hand, suggest that denoising can be done using only the noisy measurement. In other words, during model training, the image itself acts as the target image.

One issue that could arise at this step is that the model could converge to an identity function. Noise2Self study proposes a form of perturbation mechanism and the J_{th} invariant principle, whereas Noise2Void study handles the denoising problem on a pixel scale and created a receptive field such that the pixel was not used during the estimation of that pixel particularly. Subsequently, studies such as [21,22] are proposed to prevent this convergence in various methods.

The opportunity of training on noisy labels could be quite valuable for low-dose CT reconstruction since it is not easy to obtain low-dose normal-dose pairs to create big datasets. Some learning methods without noise-free targets are also proposed for low-dose CT reconstruction problem. The Noise2Inverse [23] exploits Noise2Noise [18] principle by grouping projections and using them as targets against each other which exploits the statistical independency of the projections. Noise2Filter [24] study couples Noise2Inverse and NN-FBP [25] methods to train a reconstructor from a single CT image.

1.3 Contribution

In this study, Noise2Self method is adapted for the low-dose CT reconstruction problem. However, Noise2Self method may not be applied directly to low-dose CT reconstruction problem since the noise and artifacts formed during the reconstruction process are not element-wise independent. As the result, self-supervision is applied in the projection domain, where the independent noise model might be more suitable. The self-supervision is used to train a neural network that denoises the reconstructions. The proposed method outperforms both traditional and compressed sensing-based iterative reconstruction methods in the reconstruction of analytic CT phantoms and human CT

images both qualitatively and quantitatively. Furthermore, it produces results that are comparable to a well-known supervised approach, FBP+U-Net [9].

This thesis is organized as follows. The implementation and reasoning of the self-supervised training method are described in chapter 2. The experimental settings, dataset, as well as the results, are presented in chapter 3. Chapter 4 discusses the implementation details and design choices of the method. Finally, the last chapter brings the thesis to a conclusion.

2. METHOD

In this chapter, supervised and proposed self-supervised low-dose CT reconstruction methods are given. The theoretical justification of the method is provided. Besides, the details of the implementation are given.

2.1 Supervised Training for Low-Dose CT Reconstruction

The procedure for acquiring normal-dose CT images is as following:

$$y_{\mathsf{N}} = A_{\mathsf{N}} x^* + \eta, \;\; x_{\mathsf{N}} = \mathsf{FBP}(y_{\mathsf{N}}) \tag{2.1}$$

where x^* is the ground-truth x-ray attenuation of the body, A_{N} is the data acquisition matrix whose coefficients can be derived via a ray tracing algorithm, η is the data acquisition noise with zero mean, y_{N} is the normal-dose CT projections. Conventionally, the normal dose CT image is reconstructed with FBP method.

The low-dose reconstruction procedure is represented as:

$$y_{\mathsf{L}} = A_{\mathsf{L}} x^* + \eta, \;\; x_{\mathsf{L}} = \mathsf{FBP}(y_{\mathsf{L}}) \tag{2.2}$$

where x^* denotes the ground-truth image, A_{L} denotes the low-dose data acquisition matrix, y_{L} is the low-dose CT projections. Similarly, the low-dose CT image can be reconstructed with FBP method and represented here as x_{L}. However, when compared to the ground truth image, x_{L} does not usually have satisfactory image quality.

To solve low-dose CT reconstruction problem, various studies are done to find a f^* method which can be used instead of FBP to reconstruct images which are sufficiently close to x^*. Since x^* is not easy to obtain or calculate, x_{N} is usually used instead of x^*. Considering these, the optimization problem to obtain a reconstruction method can be defined as follows:

$$f^* = \min_f \mathscr{E}\{f(y_{\mathsf{L}}); x_{\mathsf{N}}\} \tag{2.3}$$

where $\mathscr{E}$ is the error function which measures the difference between the normal dose image x_{N} and the reconstructed image $f(y_{\mathsf{L}})$, y_{L} is the low-dose projections which is

defined in **(2.2)**, f is the all candidate reconstruction methods. Since it is not feasible to create all possible reconstruction methods, the reconstruction function is usually tried to be produced with deep neural networks, especially with deep CNNs. In the presence of normal-dose CT projections, a supervised reconstruction model can be defined as following:

$$\theta^* = \arg\min_{\theta} \mathbb{E}_x[\|f_\theta(x_\mathsf{L}) - x_\mathsf{N}\|_2^2] \tag{2.4}$$

where f_θ is the deep CNN which is parameterized with θ, $\mathbb{E}_x$ is the expectation over x, x_L is the reconstructed low-dose image defined in **(2.2)**, and x_N is the reconstructed normal-dose image defined in **(2.1)**. The model given in **(2.4)** can be defined in projection domain as **(2.5)**:

$$\theta^* = \arg\min_{\theta} \mathbb{E}_y[\|A_\mathsf{N} f_\theta(x_\mathsf{L}) - y_\mathsf{N}\|_2^2] \tag{2.5}$$

where $\mathbb{E}_y$ is the expectation over y random variable which represents different projections, A_N is the normal dose forward operator, x_L is the input of the system which is low-dose CT image and y_N is the target normal-dose projections. In the supervised setting, low-dose/normal-dose pairs of the same information is required and f_θ learns a mapping from low-dose to normal-dose one.

2.2 Self Supervised Training for Low-Dose CT Reconstruction

In the previous sub-chapter, how a supervised method can work for low-dose CT problem is given. However, due to the sensitivity of human tissues to ionizing radiation, acquiring such low-dose/normal-dose pairs is challenging. In this manner, the proposed method requires only the low-dose projections y_L and does not require y_N or x_N. This framework is proposed by defining a self-supervised loss that only utilizes low-dose projections and images, y_L and x_L.

$$\mathbb{E}_{x,y}[\|A_\mathsf{L} f_\theta(x_\mathsf{L}) - y_\mathsf{L}\|_2^2] \tag{2.6}$$

where $\mathbb{E}_{x,y}$ is expectation over x and y random variables and the remaining terms of the equation are defined in **(2.1)** and **(2.2)**. It can be shown that the proposed self-supervised loss converges to the supervised solution, in the following part. Using **(2.2)**, y_L in **(2.6)** can be substituted with $A_\mathsf{L}x^* + \eta$:

$$\mathbb{E}_{x,n}[\|A_\mathsf{L} f_\theta(x_\mathsf{L}) - A_\mathsf{L}x^* - \eta\|_2^2] \tag{2.7}$$

The following equation can be derived by expanding the square term in **(2.7)**.

$$\theta^* = \arg\min_{\theta} \Big\{ \mathbb{E}_x[\|(A_{\mathsf{L}} f_\theta(x_{\mathsf{L}}) - A_{\mathsf{L}} x^*)\|_2^2] \; + \; \mathbb{E}_\eta[\|\eta\|_2^2] \\ - \mathbb{E}_{x,\eta}[2\langle A_{\mathsf{L}} f_\theta(x_{\mathsf{L}}) - A_{\mathsf{L}} x^*, \eta\rangle] \Big\} \tag{2.8}$$

The second term is the expectation over η of $\|\eta\|_2^2$ which can be calculated as the variance of the noise and not taken into account during the minimization since the self-supervision is applied in the projection domain where the noise and projection are considered to be independent. The third term of the equation is expectation over x, η of $-\mathbb{E}_{x,\eta}[2\langle A_{\mathsf{L}}(f_\theta(x_{\mathsf{L}}) - x^*), \eta\rangle]$ whose weight becomes minimal in **(2.8)** since $f_\theta(x_{\mathsf{L}}) - x^*$ ideally converges to zero. Furthermore, $f_\theta(x_{\mathsf{L}}) - x^*$ and η can be assumed to be independent. As a result, the first term, $\mathbb{E}_x[\|(A_{\mathsf{L}} f_\theta(x_{\mathsf{L}}) - A_{\mathsf{L}} x^*)\|_2^2]$, becomes the most impactful term in this optimization problem which is actually correlated with the supervised loss defined in **(2.4)** and uses x^* as target random variable.

The reason why the self-supervised loss can be a decent candidate to learn a mapping from low-dose to normal-dose is given above. However, the problem of **(2.6)** is that f_θ might converge to an identity function. To address this issue, J_{th} invariant principle is exploited [19] which proposes that the J_{th} subset of the pixels are selected from x and they are perturbed using the neighbor pixels, and the loss is defined based on only these pixels as in **(2.9)**. This prevents the convergence of f_θ to an identity function. To apply this principle to the proposed loss function, **(2.6)** is updated as following:

$$\theta^* = \arg\min_{\theta} \mathbb{E}_y[\|J(A_{\mathsf{L}} f_\theta(\mathsf{FBP}(y_{\mathsf{LJc}})) - y_{\mathsf{L}})\|_2^2] \tag{2.9}$$

where J is the mask which filters only the J_{th} subset of the pixels, y_{LJc} is the low-dose projections whose J_{th} subset of pixels is perturbed, y_{L} is the raw low-dose projections and A_{L} is the low-dose forward operator. Lastly, the proposed loss function can be trained on low-dose projections and does not require normal-dose images or projections.

The proposed reconstruction method's entire operating architecture is shown in Fig. 2.1. Preprocessing, training, and reconstruction are the three stages of the method. Preprocessing involves creating low-dose projections from CT images using Radon transform and additive white Gaussian noise. The acquired projection dataset is divided into two parts: training and testing. For training set projections, the J_{th} subset

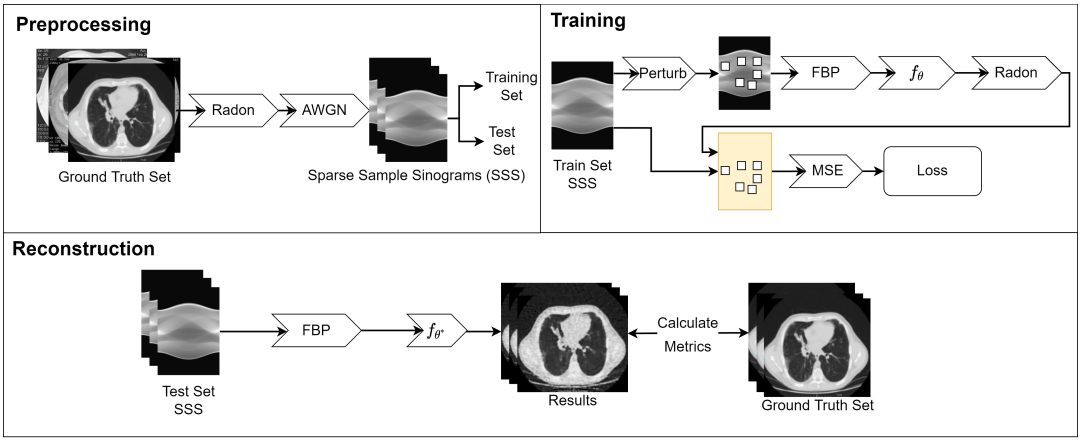

Figure 2.1 : Proposed working schema for self-supervised low-dose CT reconstruction.

of pixels is perturbed and fed into the FBP reconstruction method. The following steps are used for the perturbations:

- A grid is used to split the input image into square parts. It is set to $4x4$ in the setup.
- The pixel (i_{th}) to be perturbed is chosen by dividing the number of iterations by the number of pixels in the grid (4x4=16). For instance, if the iteration number is 172, $172 mod(16)$ is 12.
- i_{th} pixel of each grid is perturbed with the average of its four adjacent pixels, omitting the i_{th} pixel itself.

The FBP output is denoised using the neural network f_θ and then forward projected to projection domain via Radon transform. After applying the J_{th} subset mask on the error, the error is computed between the output and the perturbed projections. The neural network is optimized by using Adam [26] to minimize the loss function in **(2.9)**. The network weights (θ) are utilized for reconstruction once they have been tuned by training. During the reconstruction phase, the input projections are passed to the FBP operator in their raw form, with no modification. The proposed method denoises the FBP operator's output with the trained neural network f_{θ^*}, the output of which is the reconstructed CT image.

3. EXPERIMENTS

In this chapter the details about the experimental data, the implementation of the method and the results of the experiments are given. The experiments and the implementation are shared at the code repository[1].

3.1 Experimental Data

Both human CT data (deep lesion dataset [27]) and synthetic data (Shepp-Logan phantom and ellipses dataset) are used in this study. 512x512 pixels is chosen as the image resolution. Radon transform is used to create 64-view parallel beam projections for a simulated low-dose CT setup, and the detector resolution is adjusted to 512x1 pixels. The projections are perturbed with a random zero mean Gaussian noise of 30-40 dB.

3.2 Comparison Methods

Our self-supervised reconstruction approach is compared with FBP, SART [1], SART+TV [5], SART+BM3D [8], and a CNN based supervised reconstruction method (FBP+U-Net) [9]. For FBP, an inverse Radon transform is used with a ramp filter. SART hyperparameters are selected as iteration number=40 and relaxation parameter=0.15. The TV weight is set to 0.9, and the BM3D sigma parameter is set to 0.35. All of these hyperparameters are chosen to provide the highest PSNR values possible.

3.3 Network Architecture and Training

The denoiser neural network is built using the U-Net architecture, which is extensively used in denoising applications. FBP+U-Net [9] demonstrates why auto encoder design works well for denoising tasks such as low-dose CT reconstruction. As U-Net is an

[1] https://github.com/mozanunal/SparseCT

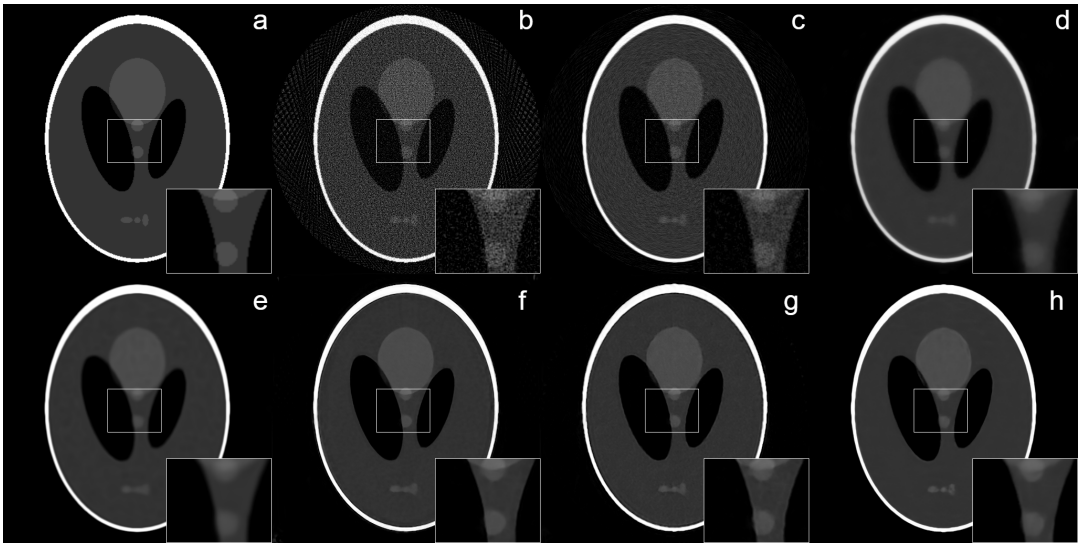

Figure 3.1 : Shepp–Logan phantom reconstruction results from 64-view projections with 37 dB noise level: a-ground truth, b-FBP, c-SART, d-SART+TV, e-SART+BM3D, f-proposed self-supervised trained on ellipses dataset, g-proposed self-supervised trained on human CT dataset, h-supervised reconstruction.

auto encoder, it is capable of extracting image features and then decoding them from latent representations. Furthermore, the gradient flow is facilitated and the higher-order structure may be transmitted to the output more efficiently due to the skip connections between the encoder and decoder scales. From the first to the final layers, the model favors a 5-scale structure with convolutional filter counts of 64, 128, 256, 512, 1024.

For both the proposed self-supervised approach and the supervised method [9], the number of parameters and training iterations are roughly 2.160.000 and 200.000, respectively. On a PC with an RTX2080 TI graphics card, the self-supervised approach is trained for 28 hours and the supervised method is trained for 24 hours. The learning rate is set to 0.0001, and Adam [26] optimizer is utilized.

We used two alternative approaches to train proposed self-supervised method: *i)* the proposed self-supervised method trained on ellipses dataset, *ii)* the proposed self-supervised method trained on human CT dataset. In the comparisons of synthetic and human CT data, each is used.

3.4 Results

For both human CT and synthetic datasets, the proposed method is evaluated with FBP, SART [1], SART+TV [5], SART+BM3D [8] and a CNN based supervised

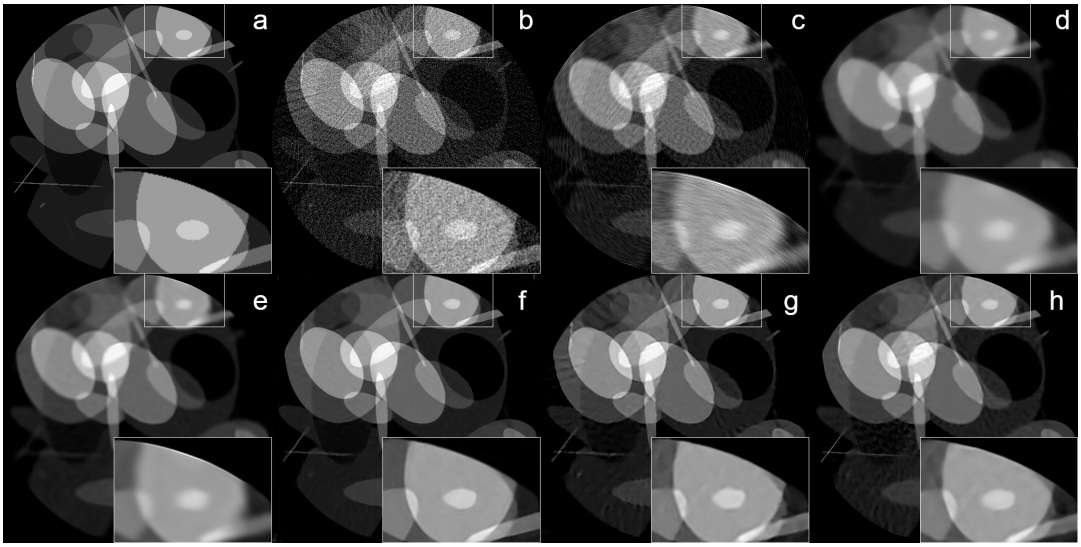

Figure 3.2 : Ellipses image reconstruction results from 64-view projections with 33 dB noise level: a-ground truth, b-FBP, c-SART, d-SART+TV, e-SART+BM3D, f-proposed self-supervised trained on ellipses dataset, g-proposed self-supervised trained on human CT dataset, h-supervised reconstruction.

Table 3.1 : Ellipses dataset reconstruction results

	30dB SNR		33dB SNR		37dB SNR	
	PSNR	SSIM	PSNR	SSIM	PSNR	SSIM
FBP	12.14 ± 1.66	0.25 ± 0.01	14.97 ± 1.62	0.29 ± 0.02	18.52 ± 1.54	0.38 ± 0.03
SART	19.38 ± 1.62	0.41 ± 0.04	21.76 ± 1.56	0.50 ± 0.05	24.36 ± 1.61	0.63 ± 0.05
SART+TV	27.59 ± 1.93	0.85 ± 0.03	27.84 ± 1.95	0.87 ± 0.03	27.99 ± 1.97	0.88 ± 0.02
SART+BM3D	27.95 ± 2.08	0.90 ± 0.03	28.36 ± 1.76	0.92 ± 0.01	28.54 ± 1.85	0.92 ± 0.01
Proj2Proj.	28.12 ± 1.70	0.91 ± 0.02	28.45 ± 2.01	0.91 ± 0.02	28.70 ± 1.94	0.92 ± 0.02
FBP+U-Net	30.48 ± 1.80	0.93 ± 0.02	31.27 ± 1.79	0.94 ± 0.01	31.90 ± 1.85	0.95 ± 0.01

reconstruction method (FBP+U-Net) [9]. PSNR and SSIM measures are used for quantitative evaluation, and visual examination is used for qualitative evaluation.

The quantitative performance of reconstruction methods using 64-view CT projections from the ellipses dataset at different noise levels is summarized in Table 3.1. The winner is highlighted in red while the runner-up is highlighted in blue. For all noise levels, FBP delivers the worst outcomes based on these criteria. When SART's output image is denoised through TV or BM3D, its performance is greatly enhanced. Under these experiment settings, the supervised method produces the best result.

Fig. 3.1 shows the reconstructions of Shepp–Logan phantom [28]. There are severe artifacts in the FBP reconstruction. SART produces better results, however there is still a lot of background noise. Although TV and BM3D efficiently suppress background noise, their over-smoothing impact reduces the detectability of tiny

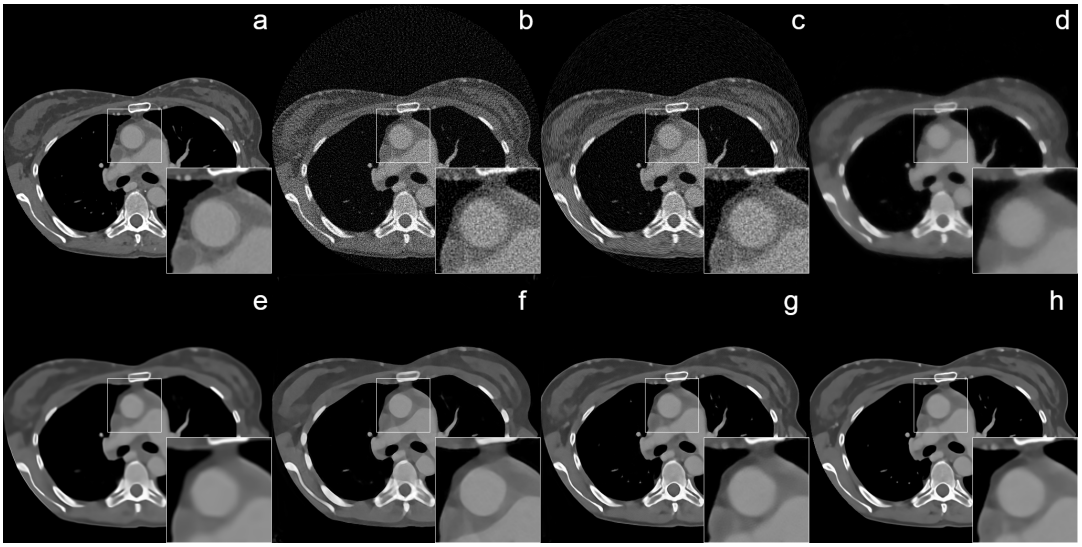

Figure 3.3 : Human CT image reconstruction results from 64-view with 37 dB SNR noise level: a-ground truth, b-FBP, c-SART, d-SART+TV, e-SART+BM3D, f-proposed self-supervised trained on ellipses dataset, g-proposed self-supervised trained on human CT dataset, h-supervised reconstruction.

features. The proposed self-supervised methods and supervised approach outperform all of the others in terms of reducing background noise and recovering the fine details. Since Shepp–Logan phantom and the ellipses dataset have similar patterns, the self-supervised approach trained on the ellipses dataset produces slightly better results than the one trained on the human CT dataset. We zoomed in on Fig. 3.1 for a better qualitative comparison between the proposed method and the supervised method, which shows that the proposed method recovers the features sharper.

Figure 3.2 shows the reconstruction results of an ellipses image. When the results of all approaches are examined, it can be found that there is a strong analogy with those obtained from the Shepp–Logan phantom in Fig. 3.1. The proposed method trained on the ellipses dataset outperforms the supervised method in suppressing background noise and recovering morphological features. Since the proposed method's network is trained using the ellipses dataset, this outcome is predicted.

The quantitative performance of reconstruction methods using 64-view CT projections from a human CT dataset at various noise levels is summarized in Table 3.2. The winner is highlighted in red while the runner-up is highlighted in blue. The proposed self-supervised approach outperforms the state-of-the-art regularized iterative algorithms. In terms of PSNR and SSIM values, the supervised method

Table 3.2 : Human CT dataset results

	30dB SNR		33dB SNR		37dB SNR	
	PSNR	SSIM	PSNR	SSIM	PSNR	SSIM
FBP	15.03 ± 1.16	0.30 ± 0.02	17.51 ± 0.95	0.36 ± 0.02	20.28 ± 0.63	0.44 ± 0.02
SART	22.20 ± 1.03	0.51 ± 0.04	24.29 ± 0.79	0.62 ± 0.04	26.04 ± 0.82	0.86 ± 0.01
SART+TV	25.95 ± 0.80	0.84 ± 0.01	26.02 ± 0.81	0.85 ± 0.01	26.16 ± 0.83	0.91 ± 0.01
SART+BM3D	27.12 ± 0.73	0.90 ± 0.01	28.20 ± 0.81	0.92 ± 0.01	28.31 ± 0.79	0.93 ± 0.01
Proj2Proj.	28.29 ± 0.93	0.92 ± 0.01	28.38 ± 0.96	0.92 ± 0.01	28.44 ± 0.98	0.93 ± 0.01
FBP+U-Net	34.07 ± 1.01	0.97 ± 0.01	35.09 ± 1.07	0.97 ± 0.01	36.14 ± 1.13	0.98 ± 0.01

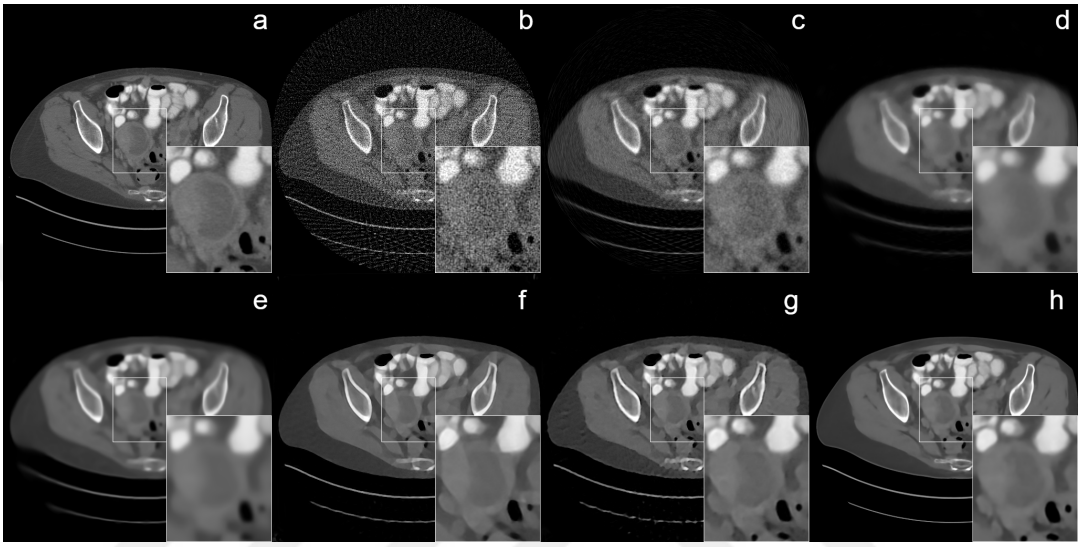

Figure 3.4 : Human CT image reconstruction results from 64-view 33 dB SNR noise level: a-ground truth, b-FBP, c-SART, d-SART+TV, e-SART+BM3D, f-proposed self-supervised trained on ellipses dataset, g-proposed self-supervised trained on human CT dataset, h-supervised reconstruction.

outperforms the proposed method significantly. However, these metrics cannot be used as a single reference for high-quality CT reconstruction. It is worth noting that these metrics are totally dependent on the accuracy of ground truth images. In CT imaging, the reference images obtained from normal-dose CT scans, on the other hand, by their very nature contain noise and artifacts. The supervised method learns a mapping from low-dose to normal-dose images that includes all of these imperfections. This could cause the supervised approach to provide very high PSNR and SSIM scores, even if the reconstruction quality may not be the best.

The findings of a human CT image reconstruction are shown in Fig. 3.3. The proposed approach and the supervised method outperform the other methods in terms of recovering fine details and removing artifacts. The proposed method, which is trained on human CT data, outperforms the one trained on the ellipses dataset, which

Table 3.3 : The execution times of the reconstructions in seconds

FBP	SART	SART+TV	SART+BM3D	Prop.	Selfsuper	Supervised
0.38	34.16	36.91	41.95	1.27		1.21

nonetheless produces acceptable results despite not being trained on human CT data. Unlike the contrast in quantitative findings between the supervised and proposed methods shown in Table 3.2, the proposed method's reconstruction quality is similar to, if not better than, the supervised method's reconstruction quality.

Figure 3.4 shows the reconstruction results of a human CT image. When the reconstruction quality of all approaches are examined, it can be found a strong resemblance with the results obtained from the human CT image shown in Fig 3.3. The noise level is increased to 33 dB for this experiment, which has the biggest negative impact on the reconstruction quality of FBP. The reconstruction quality of the proposed and supervised approaches is still comparable, but the supervised method suppresses background variations better.

The reconstruction time, which is reported in Table 3.3, is another parameter that should be measured. Despite the fact that the self-supervised and supervised methods take a long time to train, thanks to modern computing technology, the forward propagation times for trained neural networks are rather short.

4. DISCUSSION

In this chapter, detailed information about the design choices and limitations of the study are given.

In the proposed method, the noise reduction is preferred to be done in the image domain. Even though there are some studies which are focused on the projection denoising and compilation [29, 30], the number of studies which are using CNNs in image domain is far superior. Therefore, image domain supervised denoiser method is selected for a fair comparison. In addition, [31] states that the structure of deep CNNs are fine-tuned for natural images, and they can generate natural images easier than noise.

Another point of discussion in terms of putting the proposed approach into practice is whether FBP should be used as the initial reconstruction method. FBP, the most common reconstruction method, is utilized in FBP+U-Net, and an architecture that is similar to FBP+U-Net [9] is chosen for a fair comparison in the experiments. Iterative or regularized iterative approaches for the initial reconstruction, on the other hand, may aid in obtaining better outcomes. Due to its network design and initial reconstruction technique, FBP+U-Net is considered to be one of the best and most fair options to be used in the comparisons among several supervised low-dose CT reconstruction methods.

One of the limitations of the experiments is the simulated projections. The real projections can suffer from some other physical effects like scattering and Poisson noise. In the experiments, the sparse view simulated projections are created via Radon transform with additive Gaussian noise from real CT images which are already exposed to these physical effects and signal dependent Poisson noise.

The convergence of the network weights to an identity function is one of the problems of the proposed training approach. To address this issue, the J_{th} invariance approach suggested in Noise2Self [19] study is employed which executes pixel-based denoising while assuming inter-pixel noise independency. Due to the back projection operator,

noise in a low-dose CT image cannot be modeled independently on a pixel-by-pixel basis. To overcome that, J_{th} invariance approach is used in the projection domain, where the noise may be represented independent pixel by pixel. In addition, the network converges to an identity function when the self-supervision principle is tested in the image domain, leading in a result that is almost identical to the output of the FBP operator.

5. CONCLUSIONS

In conclusion, the availability of large labeled dataset for low-dose CT problem is quite limited. In this study, a novel training scheme is proposed which uses only the low-dose projection data without the need of low-dose/normal-dose pairs. The proposed method gives way better results than the regularized iterative methods and comparable results with a recent supervised method [9] both qualitatively and quantitatively. This method can also be applied to other biomedical inverse imaging problems where the ground truth data is not available and the assumptions used in this study are applicable. For the future studies, its potential for other inverse imaging problems and the clinical usability of the method can be explored.

REFERENCES

[1] **Andersen, A. and Kak, A.** (1984). Simultaneous Algebraic Reconstruction Technique (SART): A superior implementation of the ART algorithm, *Ultrasonic Imaging*, *6*(1), 81 – 94, http://www.sciencedirect.com/science/article/pii/0161734684900087.

[2] **Donoho, D.L.** (2006). Compressed sensing, *IEEE Transactions on Information Theory*, *52*(4), 1289–1306.

[3] **Candès, E.**, **Romberg, J. and Tao, T.** (2006). Stable Signal Recovery from Incomplete and Inaccurate Measurements, *Communications on Pure and Applied Mathematics*, *59*.

[4] **Rudin, L.I.**, **Osher, S. and Fatemi, E.** (1992). Nonlinear total variation based noise removal algorithms, *Physica D: Nonlinear Phenomena*, *60*(1), 259 – 268, http://www.sciencedirect.com/science/article/pii/016727899290242F.

[5] **Yu, H. and Wang, G.** (2009). Compressed sensing based interior tomography, *Physics in medicine & biology*, *54*(9), 2791.

[6] **Sidky, E.Y. and Pan, X.** (2008). Image reconstruction in circular cone-beam computed tomography by constrained, total-variation minimization, *Physics in Medicine and Biology*, *53*(17), 4777–4807, https://doi.org/10.1088%2F0031-9155%2F53%2F17%2F021.

[7] **Buades, A.**, **Coll, B. and Morel, J.M.** (2005). A non-local algorithm for image denoising, *2005 IEEE Computer Society Conference on Computer Vision and Pattern Recognition (CVPR'05)*, volume 2, pp.60–65 vol. 2.

[8] **Dabov, K.**, **Foi, A.**, **Katkovnik, V. and Egiazarian, K.** (2007). Image Denoising by Sparse 3-D Transform-Domain Collaborative Filtering, *IEEE Transactions on Image Processing*, *16*(8), 2080–2095.

[9] **Jin, K.H.**, **McCann, M.T.**, **Froustey, E. and Unser, M.** (2017). Deep Convolutional Neural Network for Inverse Problems in Imaging, *IEEE Transactions on Image Processing*, *26*(9), 4509–4522.

[10] **Chen, H.**, **Zhang, Y.**, **Kalra, M.K.**, **Lin, F.**, **Chen, Y.**, **Liao, P.**, **Zhou, J. and Wang, G.** (2017). Low-Dose CT With a Residual Encoder-Decoder Convolutional Neural Network, *IEEE Transactions on Medical Imaging*, *36*(12), 2524–2535.

[11] **Buzug, T.** (2008). *Computed Tomography : From Photon Statistics to Modern Cone-Beam CT*.

[12] **Yang, Q.**, **Yan, P.**, **Zhang, Y.**, **Yu, H.**, **Shi, Y.**, **Mou, X.**, **Kalra, M.K.**, **Zhang, Y.**, **Sun, L. and Wang, G.** (2018). Low-Dose CT Image Denoising Using a Generative Adversarial Network With Wasserstein Distance and Perceptual Loss, *IEEE Transactions on Medical Imaging*, *37*(6), 1348–1357.

[13] **Liu, Z.**, **Bicer, T.**, **Kettimuthu, R.**, **Gursoy, D.**, **Carlo, F.D. and Foster, I.** (2020). TomoGAN: low-dose synchrotron x-ray tomography with generative adversarial networks: discussion, *J. Opt. Soc. Am. A*, *37*(3), 422–434, `http://josaa.osa.org/abstract.cfm?URI=josaa-37-3-422`.

[14] **Adler, J. and Öktem, O.** (2018). Learned Primal-Dual Reconstruction, *IEEE Transactions on Medical Imaging*, *37*(6), 1322–1332.

[15] **Wu, D.**, **Kim, K.**, **El Fakhri, G. and Li, Q.** (2017). Iterative Low-Dose CT Reconstruction With Priors Trained by Artificial Neural Network, *IEEE Transactions on Medical Imaging*, *36*(12), 2479–2486.

[16] **He, J.**, **Yang, Y.**, **Wang, Y.**, **Zeng, D.**, **Bian, Z.**, **Zhang, H.**, **Sun, J.**, **Xu, Z. and Ma, J.** (2019). Optimizing a Parameterized Plug-and-Play ADMM for Iterative Low-Dose CT Reconstruction, *IEEE Transactions on Medical Imaging*, *38*(2), 371–382.

[17] **Baguer, D.O.**, **Leuschner, J. and Schmidt, M.** (2020). Computed tomography reconstruction using deep image prior and learned reconstruction methods, *Inverse Problems*, *36*(9), 094004, `https://doi.org/10.1088%2F1361-6420%2Faba415`.

[18] **Lehtinen, J.**, **Munkberg, J.**, **Hasselgren, J.**, **Laine, S.**, **Karras, T.**, **Aittala, M. and Aila, T.** (2018). Noise2Noise: Learning Image Restoration without Clean Data, *Proceedings of the 35th International Conference on Machine Learning, ICML 2018, Stockholmsmässan, Stockholm, Sweden, July 10-15, 2018*, volume 80 of *Proceedings of Machine Learning Research*, PMLR, pp.2971–2980, `http://proceedings.mlr.press/v80/lehtinen18a.html`.

[19] **Batson, J. and Royer, L.** (2019). Noise2Self: Blind Denoising by Self-Supervision, *Proceedings of the 36th International Conference on Machine Learning, ICML 2019, 9-15 June 2019, Long Beach, California, USA*, volume 97, PMLR, pp.524–533, `http://proceedings.mlr.press/v97/batson19a.html`.

[20] **Krull, A.**, **Buchholz, T. and Jug, F.** (2019). Noise2Void - Learning Denoising From Single Noisy Images, *IEEE Conference on Computer Vision and Pattern Recognition, CVPR 2019, Long Beach, CA, USA, June 16-20, 2019*, Computer Vision Foundation / IEEE, pp.2129–2137, `http://openaccess.thecvf.com/content_CVPR_2019/html/Krull_Noise2Void_-_Learning_Denoising_From_Single_Noisy_Images_CVPR_2019_paper.html`.

[21] **Quan, Y.**, **Chen, M.**, **Pang, T. and Ji, H.** (2020). Self2Self With Dropout: Learning Self-Supervised Denoising From Single Image, *2020 IEEE/CVF Conference on Computer Vision and Pattern Recognition (CVPR)*, pp.1887–1895.

[22] **Xie, Y.**, **Wang, Z. and Ji, S.** (2020). Noise2Same: Optimizing A Self-Supervised Bound for Image Denoising, ***H. Larochelle***, ***M. Ranzato***, ***R. Hadsell***, ***M. Balcan and H. Lin***, *editors, Advances in Neural Information Processing Systems 33: Annual Conference on Neural Information Processing Systems 2020, NeurIPS 2020, December 6-12, 2020, virtual*, `https://proceedings.neurips.cc/paper/2020/hash/ea6b2efbdd4255a9f1b3bbc6399b58f4-Abstract.html`.

[23] **Hendriksen, A.A.**, **Pelt, D.M. and Batenburg, K.J.** (2020). Noise2Inverse: Self-Supervised Deep Convolutional Denoising for Tomography, *IEEE Transactions on Computational Imaging*, *6*, 1320–1335.

[24] **Lagerwerf, M.J.**, **Hendriksen, A.A.**, **Buurlage, J.W. and Batenburg, K.J.**, (2020), Noise2Filter: fast, self-supervised learning and real-time reconstruction for 3D Computed Tomography, `2007.01636`.

[25] **Pelt, D.M. and Batenburg, K.J.** (2013). Fast Tomographic Reconstruction From Limited Data Using Artificial Neural Networks, *IEEE Transactions on Image Processing*, *22*(12), 5238–5251.

[26] **Kingma, D.P. and Ba, J.** (2015). Adam: A Method for Stochastic Optimization, *3rd International Conference on Learning Representations, ICLR 2015, San Diego, CA, USA, May 7-9, 2015, Conference Track Proceedings*, `http://arxiv.org/abs/1412.6980`.

[27] **Yan, K.**, **Wang, X.**, **Lu, L. and Summers, R.M.**, (2017), DeepLesion: Automated Deep Mining, Categorization and Detection of Significant Radiology Image Findings using Large-Scale Clinical Lesion Annotations, `1710.01766`.

[28] **Shepp, L.A. and Logan, B.F.** (1974). The Fourier reconstruction of a head section, *IEEE Transactions on Nuclear Science*, *21*(3), 21–43.

[29] **Lee, H.**, **Lee, J.**, **Kim, H.**, **Cho, B. and Cho, S.** (2019). Deep-Neural-Network-Based Sinogram Synthesis for Sparse-View CT Image Reconstruction, *IEEE Transactions on Radiation and Plasma Medical Sciences*, *3*(2), 109–119.

[30] **Anirudh, R.**, **Kim, H.**, **Thiagarajan, J.J.**, **Mohan, K.A.**, **Champley, K. and Bremer, T.** (2018). Lose the Views: Limited Angle CT Reconstruction via Implicit Sinogram Completion, *2018 IEEE/CVF Conference on Computer Vision and Pattern Recognition*, pp.6343–6352.

[31] **Ulyanov, D.**, **Vedaldi, A. and Lempitsky, V.** (2018). Deep Image Prior, *Proceedings of the IEEE Conference on Computer Vision and Pattern Recognition (CVPR)*.

CURRICULUM VITAE

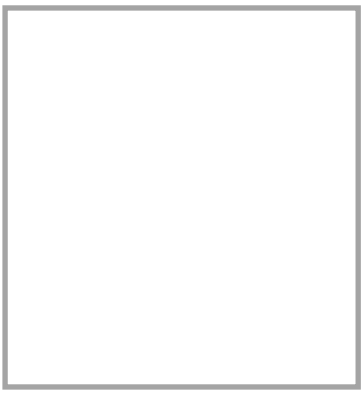

Name Surname **:** Mehmet Ozan ÜNAL

EDUCATION **:**

- **B.Sc.** **:** 2017, Istanbul Technical University, Faculty of Electrical and Electronics, Department of Electronics and Communication Engineering

PROFESSIONAL EXPERIENCE AND REWARDS:

- 2021 - Now: Senior Data Engineer at Electrolux Global Data Science, Stockholm, Sweden.
- 2019 - 2021: AI and Data Team Leader at muTech GmbH, Hannover, Germany.
- 2016 - 2019: Software Engineer at BasesTech, Istanbul, Turkey.
- 2017: Semi Finals, Digilent Design Contest, Cluj, Romania.
- 2017: 1st Place in NASA Space Apps Challenge, Istanbul, Turkey,
- 2016: Siemens Hackathon Industry 4.0, 3rd Place.
- 2016: AUVSI SUAS 13th Place as ITUNOM Unmanned Air Vehicle Team Maryland, USA.
- 2013: Participation of Intercollegiate Rocket Engineering Competition, Utah, USA.

PUBLICATIONS, PRESENTATIONS AND PATENTS ON THE THESIS:

- **Gunduzalp D., Cengiz B., Unal MO., Yildirim, I.** 2021.3D U-NetR: Low-Dose Computed Tomography Reconstruction via Deep Learning and 3 Dimensional Convolutions, *arXiv preprint arXiv:2105.14130*

- **Unal MO., Ertas M., Yildirim, I.** 2021. Self-Supervised Training For Low-Dose Ct Reconstruction. *IEEE 18th International Symposium on Biomedical Imaging (ISBI)*, April 13-16, 2021 Nice, France.

- **Unal MO., Ertas M., Yildirim, I.** 2020. An Unsupervised Reconstruction Method For Low-Dose CT Using Deep Generative Regularization Prior, *arXiv preprint arXiv:2012.06448*

OTHER PUBLICATIONS, PRESENTATIONS AND PATENTS:

- **Calisici O., Salar S., Erturk M., Kircioglu H., Bajcsy A., Unal O., Cirak T.** Determination of the time of calving in Holstein-Friesian and Simmental cows by using a novel intravaginal temperature recording smart device. *ESDAR- 23rd Annual Conference of the European Society for Domestic Animal Reproduction (ESDAR)*, September 19–22, 2019, St Petersburg, Russia.

M. O. UNAL	SELF-SUPERVISED DEEP CONVOLUTIONAL NEURAL NETWORK TRAINING FOR LOW-DOSE CT RECONSTRUCTION	2022